

Monolithic integration of capacitive sensors using a double-side CMOS MEMS post process

Chih-Ming Sun¹, Chuanwei Wang², Ming-Han Tsai¹, Hsieh-Shen Hsieh²
and Weileun Fang^{1,2}

¹ Nanoengineering and Microsystem Institute, National Tsing Hua University, Hsinchu, Taiwan, Republic of China

² Power Mechanical Engineering Department, National Tsing Hua University, Hsinchu, Taiwan, Republic of China

E-mail: fang@pme.nthu.edu.tw

Received 4 August 2008, in final form 4 November 2008

Published 10 December 2008

Online at stacks.iop.org/JMM/19/015023

Abstract

This study presents a novel double-side CMOS (complementary metal-oxide-semiconductor) post-process to monolithically integrate various capacitance-type CMOS MEMS sensors on a single chip. The CMOS post-process consists of three steps: (1) front-side bulk silicon etching, (2) backside bulk silicon etching and (3) sacrificial surface metal layers etching. Using a TSMC 2P4M CMOS process and the present double-side post-process this study has successfully integrated several types of capacitive transducers and their sensing circuits on a single chip. Monolithic integration of pressure sensors of different sensing ranges and sensitivities, three-axes accelerometers, and a pressure sensor and accelerometer are demonstrated. The measurement results of the pressure sensors show sensitivities ranging from 0.14 mV kPa⁻¹ to 7.87 mV kPa⁻¹. The three-axes accelerometers have a sensitivity of 3.9 mV G⁻¹ in the in-plane direction and 0.9 mV G⁻¹ in the out-of-plane direction; and the accelerated measurement ranges from 0.3 G to 6 G.

1. Introduction

The standard CMOS (complementary metal-oxide-semiconductor) process, offered by various commercial foundries such as TSMC (Taiwan Semiconductor Manufacturing Company), UMC (United Microelectronics Corporation), etc, has been extensively applied to fabricate MEMS devices [1]. The integration of the standard CMOS process and various CMOS post-processes for MEMS applications have been summarized in [2]. In general, the CMOS post-processes to fabricate suspended MEMS structures can be categorized into three types: (1) front-side bulk Si etching [3, 4]; (2) backside bulk Si etching [5]; and (3) surface micromachining by removing sacrificial metal films from the front-side of the Si substrate [6, 7]. CMOS MEMS processes have the advantage of monolithic integration of the integrated circuit (IC) and micromechanical components. In addition, mature CMOS fabrication processes are available in many IC foundries. CMOS-based micro fabrication technology

provides a promising approach to implement MEMS sensors. To date, various CMOS-based MEMS sensors have been reported, for instance, inertial sensors [8], chemical gas sensors [9, 10], microphones [11] and pressure sensors [7].

The integration of sensors has many applications in the automobile industry, consumer products and various other industries. For instance, the integration of a pressure sensor, temperature sensor and accelerometer is used for a smart tire pressure monitoring system (TPMS)^{3,4,5}. The pressure sensor and temperature sensor of the TPMS are respectively employed to detect the tire pressure and temperature in the wheel. The integration of an accelerometer into the TPMS detects the centrifugal force from the rotating wheel and acts as a switch to power on the TPMS system (see footnote 4).

³ Freescale semiconductor <http://www.freescale.com/>.

⁴ Freescale semiconductor, TPMS WHITE PAPER: Freescale Single-Package Tire Pressure Monitoring System (TPMS).

⁵ Infineon Technologies <http://www.infineon.com/cms/en/product/index.html>.

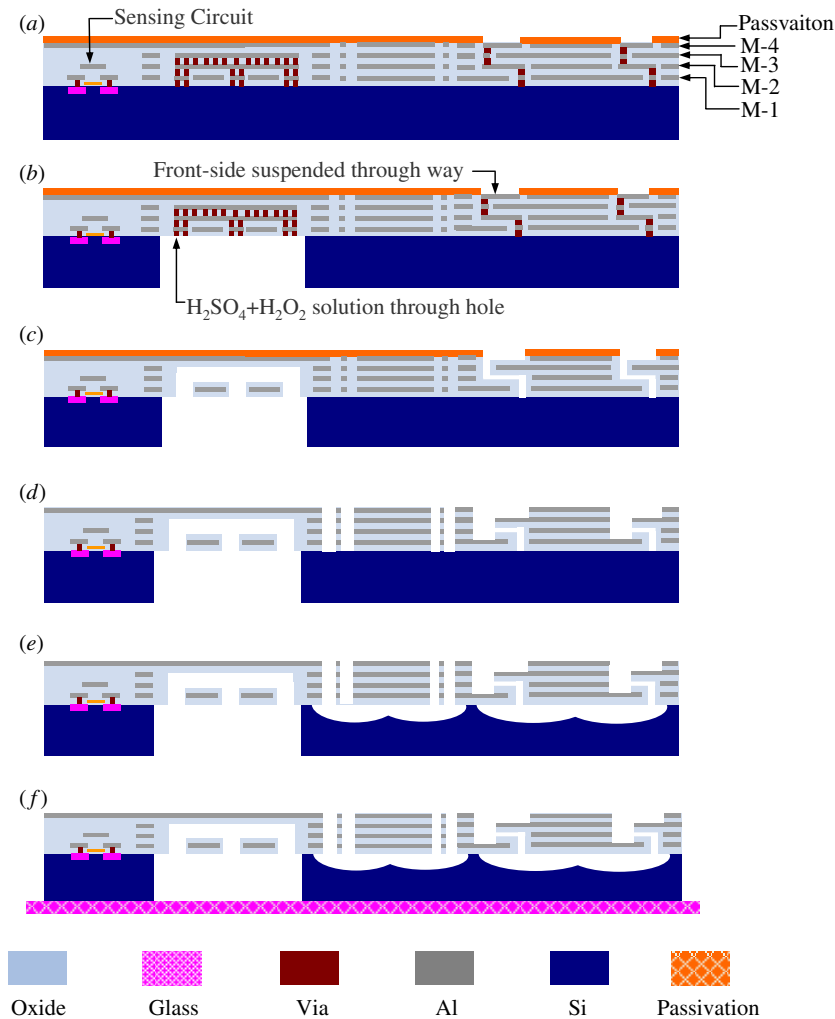


Figure 1. Fabrication steps for CMOS post-process.

An approach integrating MEMS devices with CMOS-IC using a Si wafer bonding process, and further integrating piezoresistive pressure sensors and accelerometers has been demonstrated in [12]. A silicon-on-glass (SOG) process has been used to monolithically integrate temperature, pressure and relative humidity sensors in [13]. The integration of chemical, calorimetric and mass-sensitive sensors on a single chip using the CMOS approach is reported in [14].

Although there are many available micro sensors implemented using CMOS MEMS processes, it is difficult to monolithically integrate these CMOS MEMS sensors since they have different post-processes [2]. It would be useful to establish a generic post-process platform to simultaneously implement various CMOS MEMS sensors, so as to streamline the monolithic integration of sensors. This study has integrated sacrificial metal layers etching with both front-side and backside bulk silicon etching to demonstrate a novel double-side CMOS post-process. Various capacitance-type CMOS MEMS sensors, including multi-axes accelerometers and pressure sensors of different sensitivities and sensing ranges, have been successfully fabricated and monolithically integrated on a single chip using the double-side CMOS post-process.

2. CMOS MEMS double-side post processing

This study establishes the process flow in figure 1 to fabricate and integrate various capacitance-type CMOS MEMS sensors. The chip is fabricated using the standard TSMC 0.35 μm 2P4M CMOS process. In addition to CMOS layers, the TSMC process also provides interconnect layers. Thus, as illustrated in figure 1(a), four aluminum metal films (named M-1 to M-4), four silicon dioxide dielectric films, one passivation layer, and several tungsten vias are stacked and patterned on top of the silicon substrate using the TSMC process. The present double-side post-CMOS processes are illustrated in figures 1(b)–(f). In short, these CMOS post-processes consist of: (1) front-side bulk silicon etching, (2) backside bulk silicon etching and (3) sacrificial surface metal layer etching.

As shown in figure 1(b), the backside of the silicon substrate is etched by DRIE (deep reactive ion etching) to expose the thin film layers. An aluminum film patterned using lift-off acts as the etching mask during DRIE. After that, the tungsten vias and aluminum films are employed to act as the sacrificial layers [6, 7]. Etching solution composed of H_2SO_4 and H_2O_2 is used to etch through these sacrificial layers from the backside to form suspended mechanical structures and

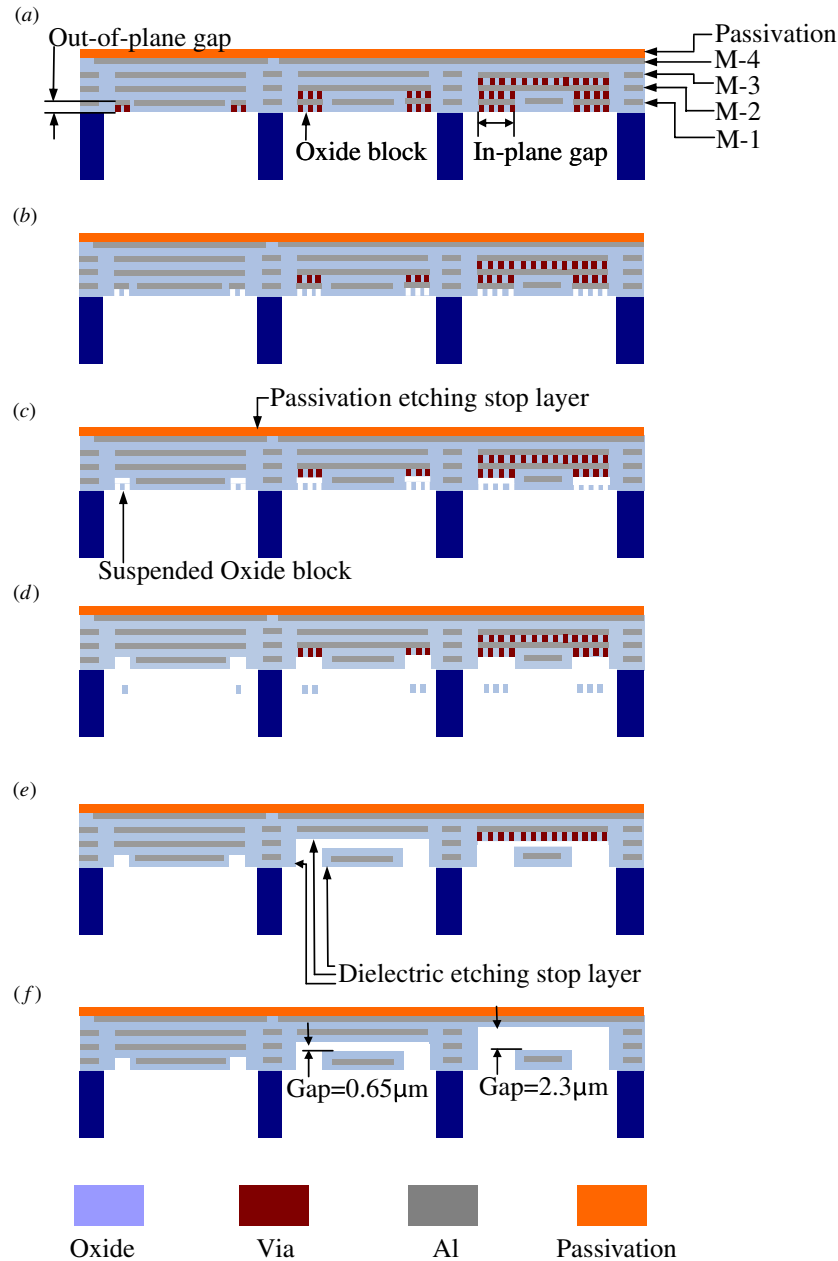


Figure 2. Detailed process steps of the backside wet etching process in figure 1(c).

sensing electrodes, as shown in figure 1(c). More detailed information about etching the backside sacrificial layers will be discussed in figure 2. In the meantime, the same etching solution is also used to etch through the sacrificial layers of the aluminum and tungsten-vias from the front-side of the substrate to form the out-of-plane gap. As illustrated in figures 1(d)–(e), the existing CMOS post-process is performed on the front-side of the substrate [3]. As shown in figure 1(d), the RIE (reactive ion etching) process removes the passivation and dielectric films from the front-side of the substrate. The top metal layer (M-4) acts as the etching mask to define the planar shape of the sensors. After that, the silicon substrate is exposed in some regions. As indicated in figure 1(e), the substrate is then etched isotropically from the front-side of the substrate using XeF₂ to fully suspend the MEMS

components. For some applications, such as pressure sensors, the substrate can be further sealed with Pyrex7740 glass at the backside, as shown in figure 1(f). Thus, various CMOS MEMS sensors can be fabricated and monolithically integrated on a single chip using this double-side process.

Figure 2 shows detailed process steps of the backside etching process in figure 1(c). The pitch of tungsten-vias is filled with silicon oxide (named oxide block) by the TSMC process. In this study, the widths of the tungsten-vias and oxide blocks are all 0.5 μm to meet the TSMC design rules. Thus, the in-plane dimensions of the structures and the in-plane gap are determined by the number of tungsten-vias and oxide blocks, as shown in figure 2(a). Moreover, the out-of-plane gap is determined by the number of stacked tungsten-vias and aluminum films. H₂SO₄ and H₂O₂ etching

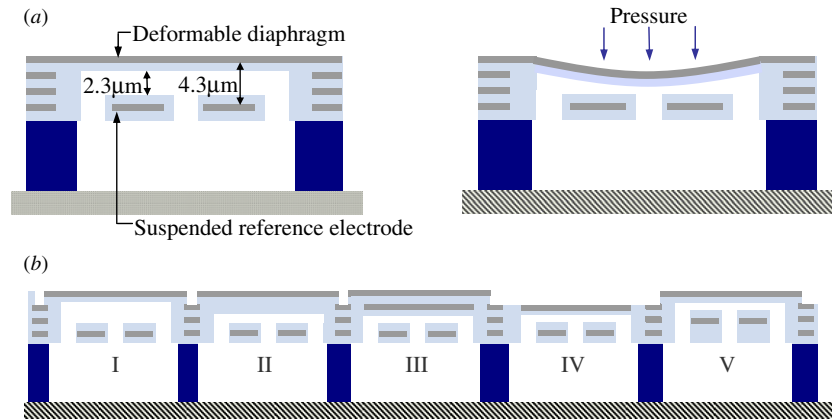


Figure 3. Design concept of the CMOS MEMS pressure sensor; (a) variation of the gap between sensing electrodes after pressure loading, and (b) pressure sensors of different sensing ranges and sensitivities.

solutions are used to remove metal films (including aluminum and tungsten). As shown in figure 2(b), the tungsten-vias are etched away, and part of the aluminum is exposed to the etching solution. After that, the exposed aluminum film is undercut until it is fully etched, as illustrated in figure 2(c). The oxide blocks surrounded by tungsten-vias and aluminum film are suspended, and as shown in figure 2(d), these suspended oxide blocks are removed from the silicon substrate. Following the same steps, the exposed tungsten-vias, oxide blocks and aluminum film could be removed, as indicated in figure 2(e). During the etching of sacrificial metal layers, the dielectric and passivation films act as the etching stop layers. Thus, in-plane and out-of-plane gaps of different sizes and patterns are fabricated after etching these sacrificial metal layers. For instance, as indicated in figure 2(f), the out-of-plane gap is defined by the M-2 and M-3 sacrificial layers, and the tungsten vias is $2.3\ \mu\text{m}$, whereas the gap defined by the M-2 sacrificial layer is only $0.65\ \mu\text{m}$. The in-plane gaps shown in figure 2(f) (from left to right) are $1.5\ \mu\text{m}$, $2.5\ \mu\text{m}$ and $3.5\ \mu\text{m}$ in width, respectively.

3. Concept of sensors design

Monolithic integrations of various capacitive type sensors, including pressure sensors of different sensing ranges and sensitivities, an in-plane accelerometer, and an out-of-plane accelerometer are employed to demonstrate the feasibility of the double-side post-process. The out-of-plane deformation of a micromachined diaphragm and the out-of-plane as well as in-plane motions of a micromachined proof-mass shown in figure 1 lead to the capacitance change of sensing electrodes. In this study, the CMOS circuits form a standard two-stage cascode differential amplifier [15], which is employed to act as the capacitance readout circuit. The CMOS circuits are monolithically integrated with the MEMS structure. Finally, the voltage output is detected using this monolithically built-in capacitance readout circuit. The design concept and sensing principle of these sensors are discussed as follows.

3.1. Pressure sensor

Figure 3(a) shows schematic illustrations of the capacitance-type pressure sensor design in this study. This device is mainly realized using the backside post-process. The present pressure sensor consists of a diaphragm and suspended structures, both of which have embedded sensing electrodes and are formed by dielectric and metal films of the CMOS process. The metal films of the CMOS process act as sensing electrodes. The diaphragm and its embedded sensing electrode (named deformable electrode) are deformed by the pressure load. On the other hand, the suspended structure and its embedded sensing electrode (named reference electrode) can be deformed by the pressure load. As a result, the pressure difference on both sides of the diaphragm leads to a gap and a capacitance change between the sensing electrodes. The pressure sensor illustrated in figure 3(a) employs M-1 and M-4 aluminum films to act as the reference and deformable electrodes, respectively. The two metal layers are covered with dielectric SiO_2 films to prevent electrical short circuiting of the sensing electrodes.

The characteristics and sensitivity of the pressure sensor in figure 3(a) vary with the diaphragm stiffness and the gap between the sensing electrodes. The stiffer diaphragm endures higher pressure loading without large nonlinear deformation or damage. As indicated in figure 3(b), various diaphragm thicknesses and sensing gaps are created by designing the stacking of metal films and the locations of tungsten plugs of the CMOS process. Therefore, the sensing range and sensitivity of the pressure sensor can be changed by the present processes. According to the TSMC $0.35\ \mu\text{m}$ 2P4M CMOS process, the diaphragm thickness for sensor-I as indicated in both figures 3(a) and (b) is $1.92\ \mu\text{m}$. The distance between the M-1 and M-4 electrodes is $4.3\ \mu\text{m}$, and the gap between the diaphragm and reference electrode is $2.3\ \mu\text{m}$. As a comparison, sensor-II in figure 3(b) also employs M-1 (reference electrode) and M-4 layers (deformable electrode) to act as the sensing electrodes. Sensor-II uses only the M-2 layer (whereas sensor-I employs both M-2 and M-3 layers) to define the gap between the diaphragm and the reference electrode.

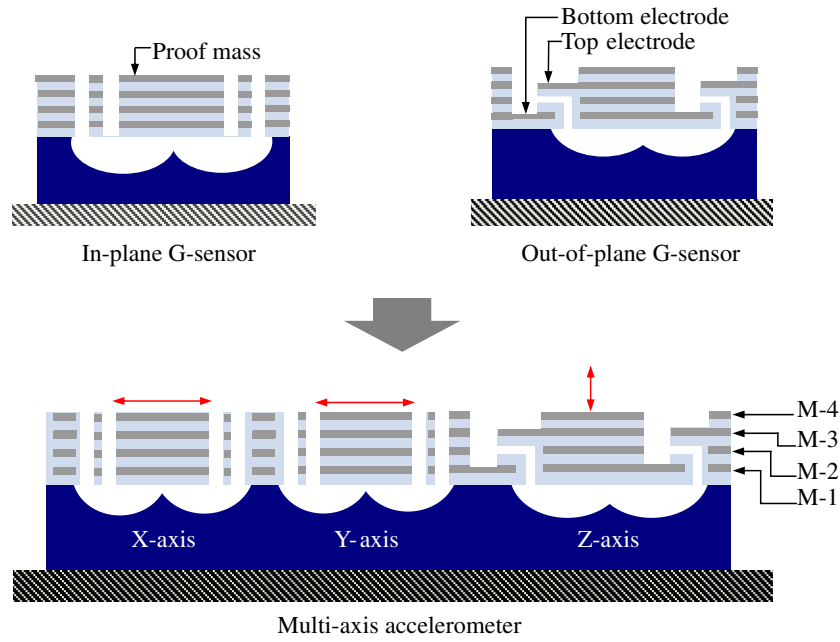


Figure 4. Design concept of the monolithic three-axis accelerometer.

Table 1. Characteristics of the CMOS MEMS pressure sensors in figure 3(b).

| | Sensor-I | Sensor-II | Sensor-III | Sensor-IV | Sensor-V |
|---------------------------------|--------------------|--------------------|--------------------|--------------------|--------------------|
| | | | | | |
| Diaphragm thickness | 1.92 μm | 3.56 μm | 3.56 μm | 1.64 μm | 1.92 μm |
| Electrode Gap (E_g) | 4.3 μm | 4.3 μm | 2.65 μm | 2.65 μm | 2.65 μm |
| Structure Chamber gap (C_g) | 2.3 μm | 0.65 μm | 0.65 μm | 0.65 μm | 0.65 μm |
| Sensitivity (mV/kPa) | 3.01 | 0.14 | 0.36 | 7.87 | 7.47 |
| Non-linearity(%) | 4.95 | 0.56 | 4.76 | 5.16 | 5.78 |

Thus, sensor-II has a smaller gap yet a thicker diaphragm than sensor-I. As a result, sensor-II is more appropriate for high pressure applications. In addition, sensor-III also employs the M-2 layer to define the gap between the diaphragm and the reference electrode. However, the M-1 (stationary electrodes) and M-3 layers (deformable electrodes) are used as the sensing electrodes. Hence, sensor-III has a larger initial capacitance of sensing electrodes and a higher sensitivity. In short, the performance of the pressure sensors can be easily adjusted using the novel double-side CMOS MEMS processes. Five different pressure sensor designs shown in figure 3(b) have

been summarized in table 1. Since these pressure sensors can be simultaneously fabricated using the double-side process, pressure sensors of different sensing ranges and sensitivities can be monolithically integrated on a single chip.

3.2. In-plane and out-of-plane accelerometers

The designs of in-plane and out-of-plane CMOS MEMS accelerometers using a front-side post process have been respectively reported in [6, 16]. This study further employs these accelerometer designs to demonstrate the feasibility of the present double-side post process. In addition, this

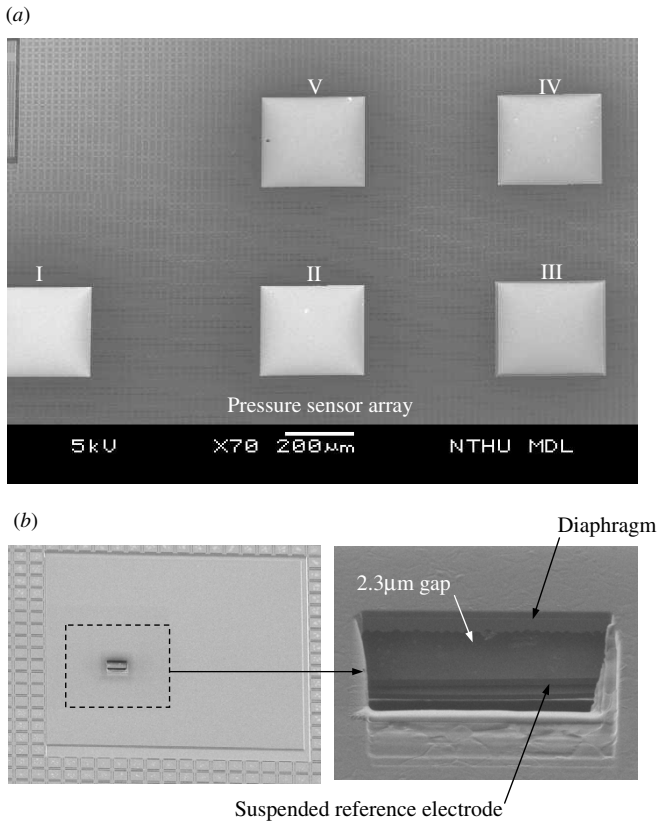


Figure 5. SEM micrographs of (a) the pressure sensor array containing five different designs, and (b) the FIB cross section of the diaphragm, sensing electrodes and gap of the pressure sensor.

study also implements a three-axes accelerometer by means of the monolithic integration of these in-plane and out-of-plane accelerometers, as shown in figure 4. The present in-plane and out-of-plane accelerometers mainly consist of a proof mass, support springs and sensing electrodes. The proof mass of the spring-mass system is excited after subsection to acceleration. The motion of the proof mass leads to the capacitance change of the sensing electrodes and determines the acceleration. Finally, the integration of the accelerometers and pressure sensors is realized using the present double-side post-process, as shown in figure 1(f).

4. Results

This study has successfully demonstrated the following three applications of sensor integration using the present double-side process: (1) pressure sensor arrays of different sensing ranges and sensitivities, (2) three axes accelerometers and (3) integration of a pressure sensor and accelerometer. The voltage outputs of these sensors are detected using the built-in capacitance readout circuits. The fabrication and measurement results of these sensors are discussed as follows.

4.1. Application I: pressure sensor arrays

The scanning electron microscope (SEM) micrograph in figure 5(a) shows the front-side view of a typical fabricated

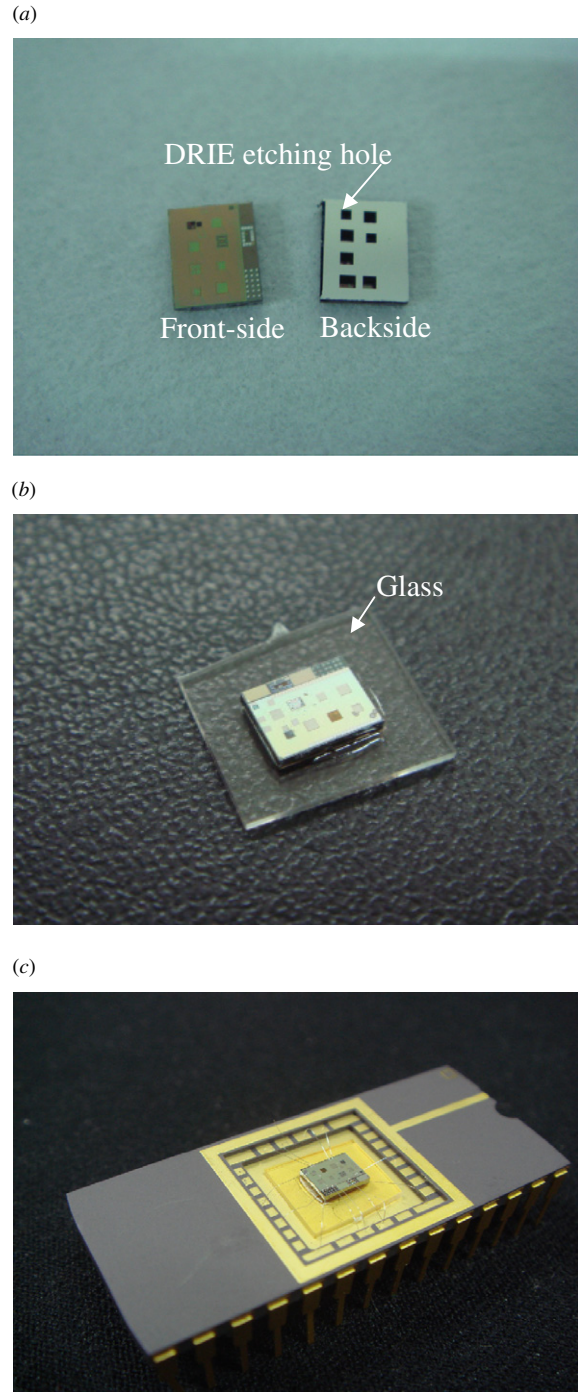


Figure 6. Photos of pressure sensor array chip (a) after fabrication, (b) after bonding with Pyrex glass and (c) after wire bonding and packaging.

chip containing five pressure sensor designs indicated in figure 3(b). The diaphragms of these five pressure sensors have the same in-plane dimensions of $300\ \mu\text{m} \times 300\ \mu\text{m}$. The SEM micrograph in figure 5(b) (left-hand side) shows the cross-section image of sensor-I prepared by FIB (focused ion beam). The zoom-in micrograph (right-hand side) clearly demonstrates the cross-sections of the diaphragm, the suspended reference electrode and the $2.3\ \mu\text{m}$ thick gap. These fabrication results demonstrate that the suspended

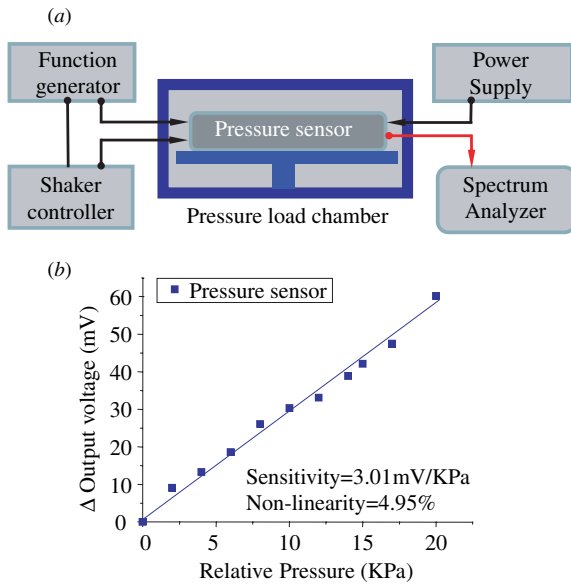


Figure 7. (a) Test setup to characterize the performances of pressure sensor and (b) the sensitivity and nonlinearity of a typical pressure sensor.

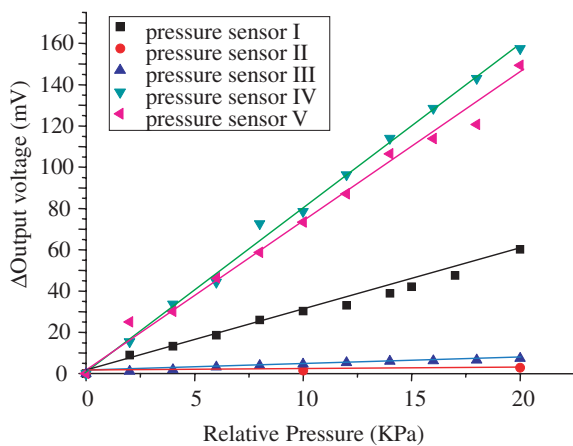


Figure 8. Measured output voltage versus pressure load for five different pressure sensor designs.

MEMS structures and sensing electrodes are successfully implemented after removing the metal and tungsten-via sacrificial layers.

The photo in figure 6(a) shows the front-side and backside views of typical fabricated chips. Holes of two different sizes etched by DRIE are observed at the backside of the substrate. Figure 6(b) further shows the bonding of the sensor chip with Pyrex glass to form a complete pressure sensing unit. The chip is shown in figure 6(c) after wire bonding and packaging inside a ceramic case. The packaged chip is used in the following pressure loading tests. Figure 7(a) shows the test setup that characterizes the performance of the pressure sensors. The sensor is placed inside a pressure chamber and the output voltage change resulting from the variation of the chamber pressure is measured by a spectrum analyzer. Limited by the test apparatus, the relative pressure load on the sensor is within the range of 20 kPa. Figure 7(b) shows the characterization

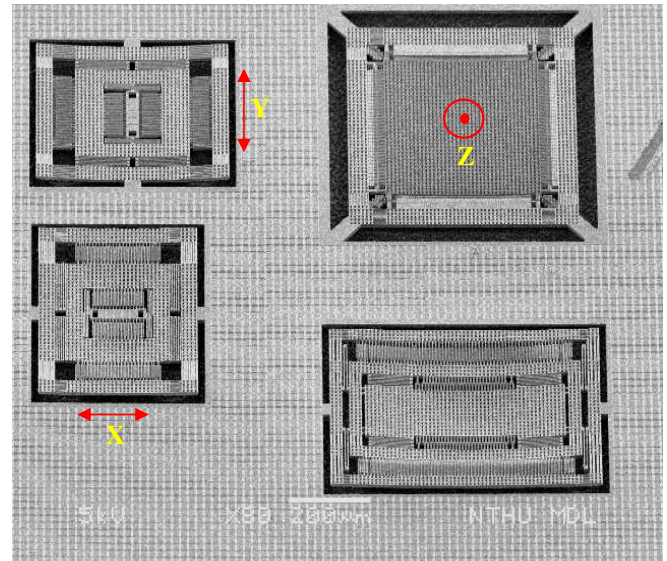


Figure 9. SEM micrograph of a typical fabricated monolithic three-axes accelerometer chip.

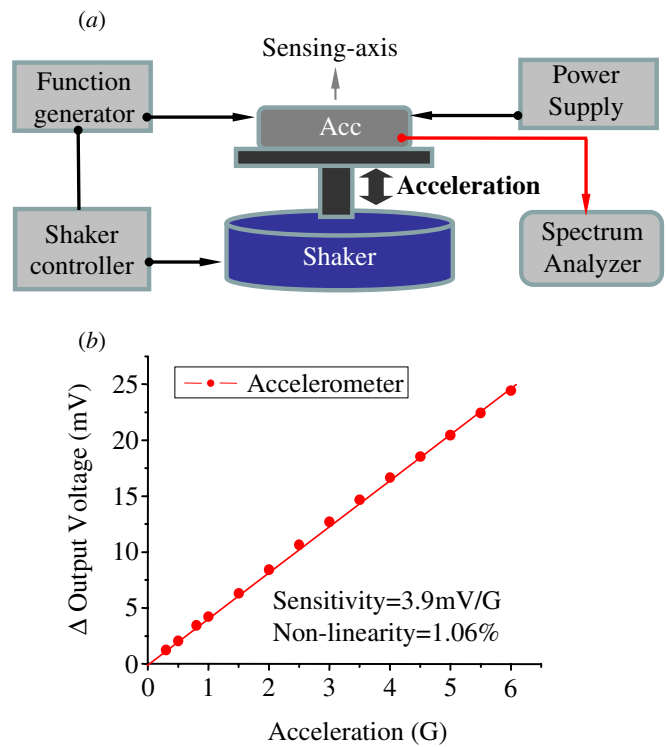


Figure 10. (a) Test setup to characterize the performances of accelerometer, and (b) sensitivity and nonlinearity of a typical accelerometer.

of output voltage versus pressure load for sensor-I shown in figure 5(a). The sensing range, sensitivity and nonlinearity of sensor-I are 0–20 kPa, 3.01 mV kPa⁻¹ and 4.95%, respectively. Figure 8 further shows the characterization of output voltage versus pressure load for the five pressure sensors indicated in figure 5(a). The performances of these five pressure sensors are summarized in table 1. The measurement results show that the sensing range and sensitivity of the pressure sensors

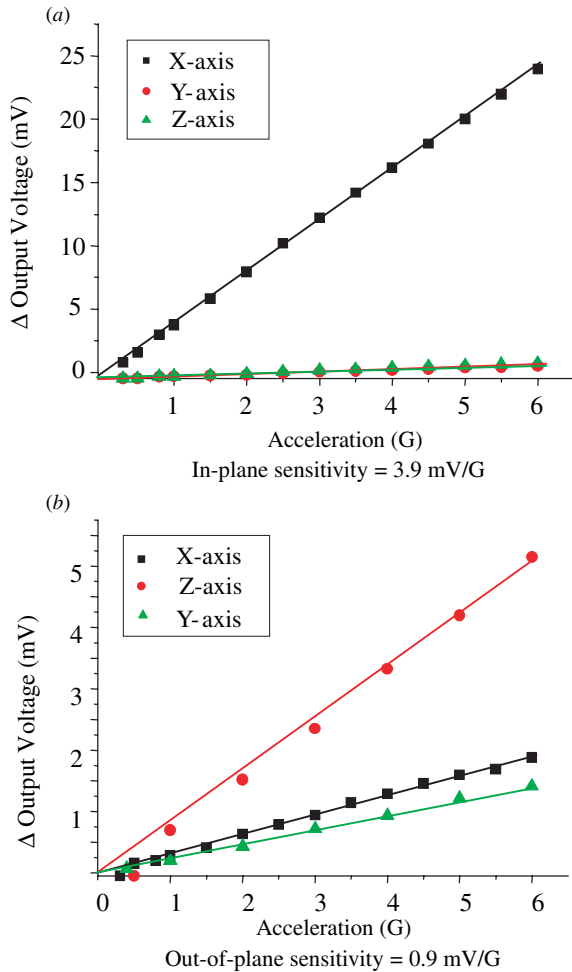


Figure 11. Measured output voltage versus acceleration for (a) in-plane (X- and Y-axes) accelerometers, and (b) out-of-plane (Z-axis) accelerometer.

can be modified using the present double-side CMOS MEMS processes.

4.2. Application II: three-axes accelerometers

The SEM micrograph in figure 9 demonstrates a typical fabricated chip containing accelerometers of three different axes, as shown in figure 4. The double-side CMOS MEMS processes successfully integrate the fully-differential capacitance sensing accelerometers reported in [6, 16]. Figure 10(a) shows the test setup to characterize the performance of three-axes accelerometers. The sensor chip was excited by a shaker, and the output voltage change of the accelerometer was measured by a spectrum analyzer. Figure 10(b) shows the typical characterization results of output voltage versus acceleration for the in-plane X-axis (or Y-axis). As a result, this three-axes accelerometer has sensitivity and nonlinearity of 3.9 mV g^{-1} and 1.06%, respectively, in its X-axis (or Y-axis). In this test, the measurement range is 0.3–6 G. Figure 11 further summarizes the measurement results of sensitivity and cross-axis sensitivity for three different axes.

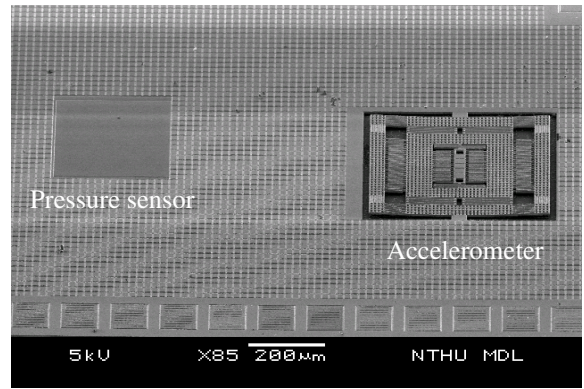


Figure 12. Front-side micrographs of the integrated pressure sensor and accelerometer chip.

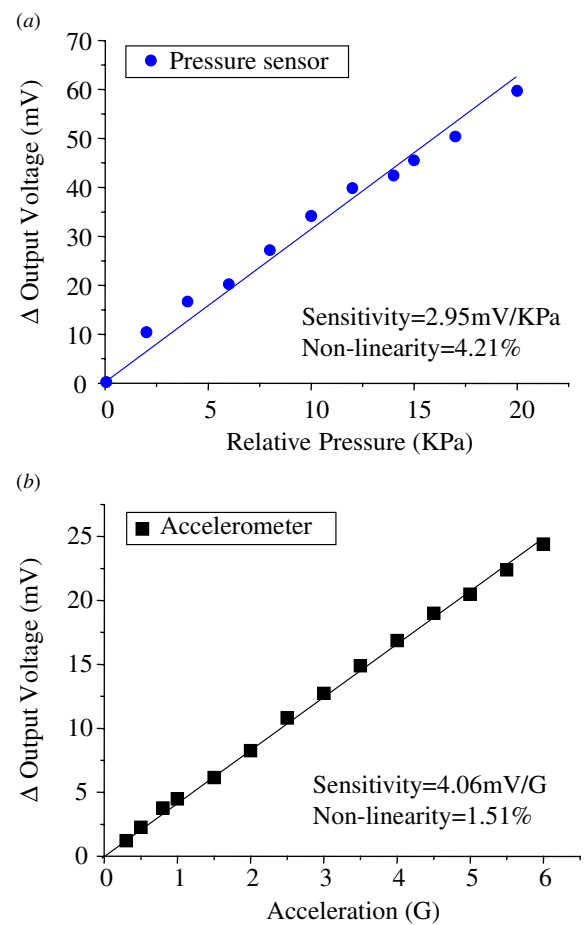


Figure 13. Characterization of the integrated pressure sensor (a) and accelerometer chip (b).

4.3. Application III: pressure sensor and G sensor

The SEM micrograph in figure 12 shows the front-side of a typical fabricated chip containing a pressure sensor and an accelerometer. The $300 \mu\text{m} \times 300 \mu\text{m}$ diaphragm of the pressure sensor is clearly observed. This pressure sensor has the same design as sensor-I. The suspended spring, proof-mass and sensing electrodes of the in-plane accelerometer are also demonstrated in the photo. The performances of

these integrated sensors are characterized using the test setups shown in figures 7(a) and 10(a). Figure 13 shows typical measurement results. The pressure sensor has a sensitivity of 2.95 mV kPa^{-1} and linearity of 4.21%, and the accelerometer has a sensitivity of 4.06 mV G^{-1} and linearity of 1.51%. These results agree well with those measured from the chips of pressure sensor arrays and three-axes accelerometers.

5. Conclusions

This study presents a double-side CMOS post-process to implement various capacitance-type CMOS MEMS sensors. Moreover, these CMOS MEMS sensors can be monolithically integrated on a single chip. The post-process mainly contains: (1) aluminum films and tungsten-vias sacrificial metal layers etching and (2) front-side and backside bulk silicon etching. To meet the CMOS process design rule, the in-plane dimensions of the suspended MEMS structures and the in-plane gaps are determined by the number of tungsten vias during the backside process. On the other hand, the out-of-plane gap is determined by the number of stacked tungsten-vias and aluminum films. The pressure sensor and accelerometer have been successfully fabricated and integrated using the TSMC $0.35 \mu\text{m}$ 2P4M CMOS process and the present double-side post-process. This study has demonstrated a chip containing five pressure sensors with different sensitivities. By varying the stacking of the metal and dielectric films, the diaphragm thickness and the stiffness of the pressure sensor are changed. The measurement results show that the sensitivity of the pressure sensors ranges from 0.14 mV kPa^{-1} to 7.87 mV kPa^{-1} . The chip containing three-axes accelerometers is also demonstrated. The three-axes accelerometers have a sensitivity of 3.9 mV G^{-1} in the in-plane directions (X - and Y -axis), and 0.9 mV G^{-1} in the out-of-plane direction (Z -axis) and a measurement range of 0.3–6 G. Finally, the integration of the accelerometer and pressure sensor has also been demonstrated. In conclusion, these capacitive type CMOS MEMS accelerometers and pressure sensors can be fabricated and monolithically integrated on a single chip using this novel double-side post-process.

Acknowledgments

This project was (partially) supported by the NSC of Taiwan under grants 96-2628-E-007-008-MY3 and 95-2218-E-007-024. The authors would like to thank TSMC Ltd, and National Chip Implementation Center (CIC), Taiwan, for supporting the IC Manufacturing. The authors would also like to thank the Center of Nano Science and Technology of National Tsing Hua

University, and the Nano Facility Center of National Chiao Tung University for providing the fabrication facilities.

References

- [1] Parameswaran M, Chung R, Gaitan M, Johnson R B and Syrzycki M 1991 Commercial CMOS fabricated integrated dynamic thermal scene simulator *IEDM'91 (Washington, DC, December 8–11)* pp 753–56
- [2] Fedder G K 2005 CMOS-based sensors *IEEE Sensors 2005 (CA, USA Oct. 30–Nov. 3)* pp 125–28
- [3] Fedder G K, Santhanam S, Reed M L, Eagle S C, Guillou D F, Lu M S-C and Carley L R 1996 Laminated high-aspect-ratio microstructures in a conventional CMOS process *Sensors Actuators A* **57** 103–10
- [4] Dai C-L, Xiao F-Y, Juang Y-Z and Chiu C-F 2005 An approach to fabricating microstructures that incorporate circuits using a post-CMOS process *J. Micromech. Microeng.* **15** 98–103
- [5] Xie H, Erdmann L, Zhu X, Gabriel K J and Fedder G K 2002 Post-CMOS processing for high-aspect-ratio integrated silicon microstructures *IEEE/ASME J. MEMS* **11** 93–101
- [6] Wang C, Tsai M-H, Sun C-M and Fang W A 2007 A novel CMOS out-of-plane accelerometer with fully-differential gap-closing capacitance sensing electrodes *J. Micromech. Microeng.* **17** 1275–80
- [7] Paul O and Baltes H 1995 Novel fully CMOS-compatible vacuum sensor *Sensors Actuators A* **46/47** 143–6
- [8] Luo H, Zhang G, Carley L R and Fedder G K 2002 A post-CMOS micromachined lateral accelerometer *IEEE/ASME J. MEMS* **11** 188–95
- [9] Graf M, Jurischka R, Barretino D and Hierlemann A 2005 3-D nonlinear modelling of microhotplates in CMOS technology for use as metal-oxide-based gas sensors *J. Micromech. Microeng.* **15** 190–200
- [10] Afridi M Y, Suehle J S, Zaghoul M E, Berning D W, Hefner A R, Cavicchi R E, Semancik S, Montgomery C B and Taylor C J 2002 A monolithic CMOS microhotplate-based gas sensor system *IEEE Sensors J.* **2** 644–55
- [11] Neumann J and Gabriel K 2002 CMOS-MEMS membrane for audio-frequency acoustic actuation *Sensors Actuators A* **95** 175–82
- [12] Parameswaran L, Hsu C and Schmidt M A 1995 A merged MEMS-CMOS. process using silicon wafer bonding *IEDM'95* pp 613–6
- [13] Dehennis A D and Wise K D 2005 A wireless microsystem for the remote sensing of pressure, temperature, and relative humidity *IEEE/ASME J. MEMS* **14** 12–22
- [14] Hagleitner C, Lange D, Hierlemann A, Brand O and Baltes H 2002 CMOS single-chip gas detection system comprising capacitive, calorimetric and mass-sensitive microsensors *IEEE J. Solid State Circuits* **37** 1867–78
- [15] Tsai J M and Fedder G K 2005 Mechanical noise-limited CMOS-MEMS accelerometers *IEEE MEMS'05 (Miami Beach, FL, Jan. 30–Feb. 3)* pp 630–3
- [16] Sun C-M, Wang C-W and Fang W 2008 On the sensitivity improvement of CMOS capacitive accelerometer *Sensors Actuators A* **141** 347–52